Int. J. Multiphase Flow Vol. 16, No. 6, pp. 1023–1045, 1990
Printed in Great Britain.

0301-9322/90 $3.00 + 0.00

FLOW REGIME TRANSITIONS DUE TO CAVITATION IN THE FLOW THROUGH AN ORIFICE

Y. YAN and R. B. THORPE†
Shell Department of Chemical Engineering, University of Cambridge, Pembroke Street, Cambridge, England

(*Received in revised form* 1 *June* 1990)

Abstract—This paper presents both experimental and theoretical aspects of the flow regime transitions caused by cavitation when water is passing through an orifice. Cavitation inception marks the transition from single-phase to two-phase bubbly flow; choked cavitation marks the transition from two-phase bubbly flow to two-phase annular jet flow.

It has been found that the inception of cavitation does not necessarily require that the minimum static pressure at the vena contracta downstream of the orifice, be equal to the vapour pressure liquid. In fact, it is well above the vapour pressure at the point of inception. The cavitation number [$\sigma = (P_3 - P_v)/(0.5\rho V^2)$; here P_3 is the downstream pressure, P_v is the vapour pressure of the liquid, ρ is the density of the liquid and V is the average liquid velocity at the orifice] at inception is independent of the liquid velocity but strongly dependent on the size of the geometry. Choked cavitation occurs when this minimum pressure approaches the vapour pressure. The cavitation number at the choked condition is a function of the ratio of the orifice diameter (d) to the pipe diameter (D) only. When super cavitation occurs, the dimensionless jet length [$L/(D - d)$; where L is the dimensional length of the jet] can be correlated by using the cavitation number. The vaporization rate of the surface of the liquid jet in super cavitation has been evaluated based on the experiments.

Experiments have also been conducted in which air was deliberately introduced at the vena contracta to simulate the flow regime transition at choked cavitation. Correlations have been obtained to calculate the critical air flow rate required to cause the flow regime transition. By drawing an analogy with choked cavitation, where the air flow rate required to cause the transition is zero, the vapour and released gas flow rate can be predicted.

Key Words: flow regime transition, cavitation, orifice, choked cavitation, super cavitation, vaporization, liquid jet

1. INTRODUCTION

Cavitation is a commonly encountered phenomenon in situations where liquids are transported through pipelines. The phenomenon is essentially a combination of the release of the dissolved gas and the vaporization of the liquid upon pressure reduction. Near inception, gas release is important, whereas at choked and in super cavitation, the vaporization of the liquid is dominant. Therefore, the mechanism of mass transfer governs the onset and development of cavitation.

A flowing system can have different flow regimes depending on the extent of cavitation. Once cavitation occurs in a flowing system, the single liquid phase first appears as a two-phase bubbly medium in the cavitation zone. As cavitation becomes more and more severe, both the size and number of cavitation bubbles are increased. The detachment or separation of the flow from the downstream side of the orifice can be observed; a phenomenon which is called choked cavitation when it is on the point of occurring, and thereafter super cavitation. A further decrease in the downstream pressure or increase in the upstream pressure leads to super cavitation: the submerged liquid jet becomes visually apparent with the vapour and the released gas surrounding the jet. The jet contains no bubbles.

The fundamental requirement for cavitation to occur is a sufficient reduction in the static pressure. To meet this requirement, the flow area in the flow passage has to change, e.g. a converging–diverging conduit, or a piece of pipe which contains a valve or an orifice.

Figure 1 shows the velocity and the pressure profiles schematically. At the vena contracta the flowing area is at its minimum and consequently, from the continuity equation, the velocity is

†To whom all correspondence should be addressed.

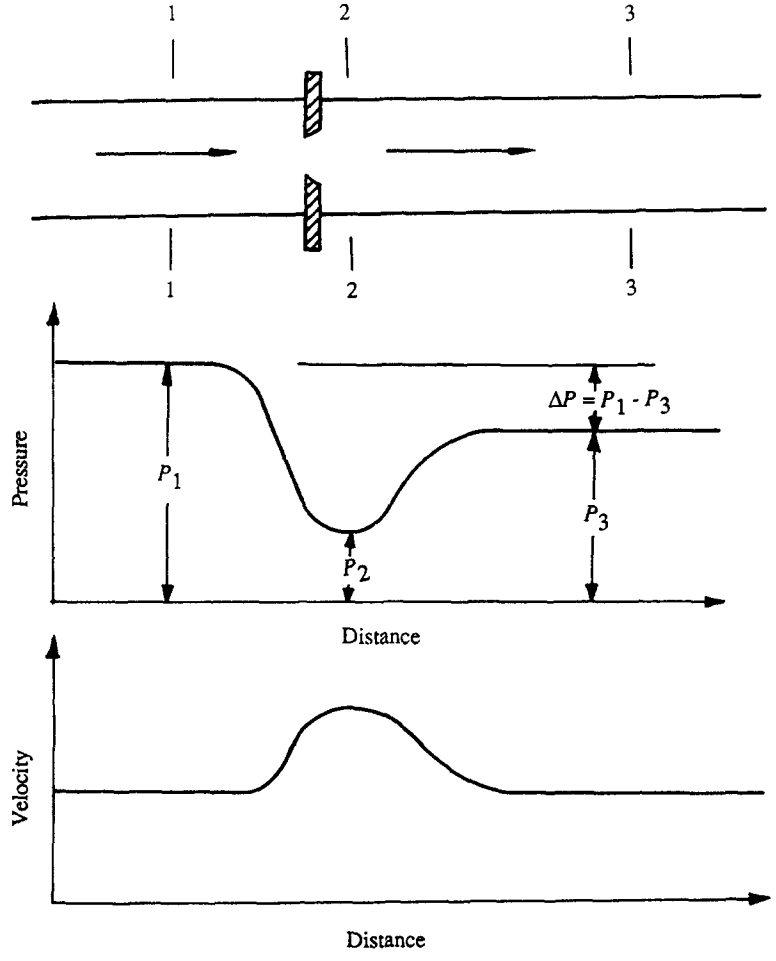

Figure 1. Pressure and velocity profiles through an orifice.

at its maximum. It follows from the energy equation that the static pressure is at its minimum. The reduction in the static pressure initializes the growth of cavitation bubbles from gas nuclei. The pressure recovery beyond the vena contracta causes the collapse of the cavitation bubbles and produces noise, an important feature of cavitation (Yan *et al.* 1988).

Early research on the flow regime transition in cavitation, i.e. cavitation inception and choked cavitation, includes that of Numachi *et al.* (1960), Tullis & Govindarajan (1973) and Ball *et al.* (1975). However, it appears that there are some inconsistencies with regard to the first transition, from single-phase to two-phase flow. On the other hand, it has not been possible to predict choked and super cavitation. In this work, attempts have been made to obtain more experimental evidence and to explore the theoretical aspects associated with the transitions. A special effort has been made to evaluate the gas and vapour flow rates at choked cavitation, and the vaporization rate at super cavitation.

2. EXPERIMENTAL SETUP

Figure 2 shows the schematic diagram of the experiment. Water was circulated through a closed circuit. The working section consists of a piece of Perspex pipe (i.d. = 3.78 cm), an orifice and a sparger which is located at the vena contracta through which air may be admitted or injected as required. The details of the sparger and a diagram of it may be found in Yan (1989). The orifice was made according to the ASME (1959) standard. The internal diameter of the inlets is 3 mm. Air is introduced through the inlets in the sparger either by being sucked into the flow if the pressure at the vena contracta was low enough or by forced injection if required. A calibrated pitot tube,

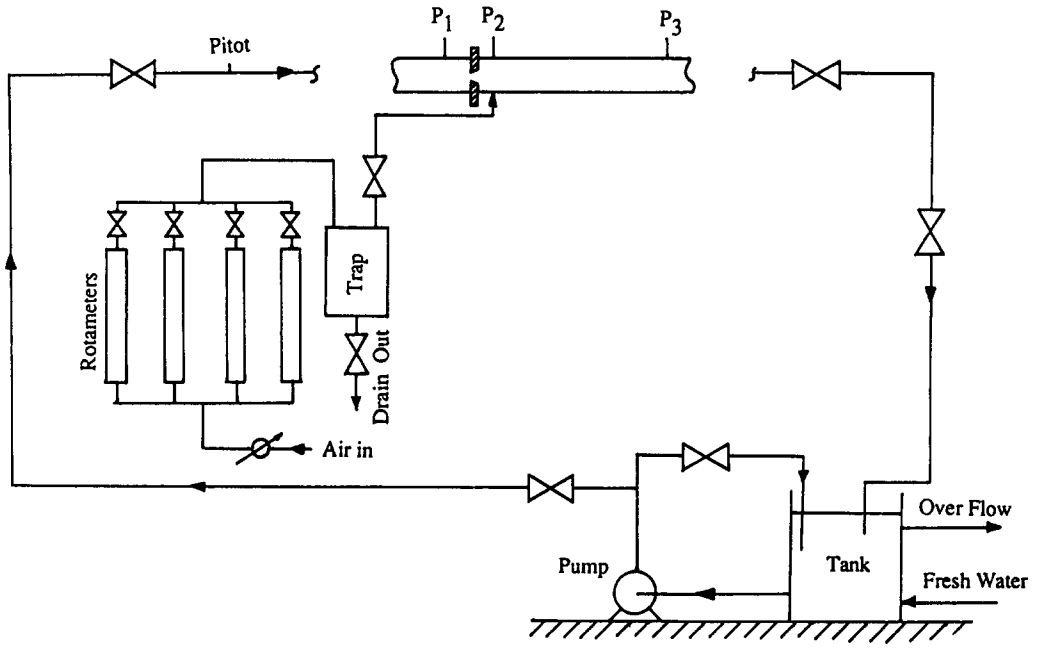

Figure 2. Schematic diagram of the experimental apparatus.

located 2 m upstream of the orifice and 2 m downstream of the valve, measures the liquid velocity in the pipe.

The pressure tapping from the upstream pressure (P_1) is located 1 pipe diameter upstream of the orifice and the downstream pressure (P_3) tapping is located 15 pipe diameters downstream. Two pressure gauges were used for the measurement of P_1 and P_3. The minimum pressure P_2 was measured at the vena contracta, the location of which is determined in accordance with ASME (1959). A manometer was used to measure P_2. Four rotameters with different ranges were utilized to measure the air flow rate.

3. TRANSITION FROM SINGLE-PHASE TO TWO-PHASE FLOW—CAVITATION INCEPTION

3.1. Cavitation Inception Number σ_i

A dimensionless parameter which has been widely used in the study of cavitation is the cavitation number, which is defined as

$$\sigma = \frac{P_3 - P_v}{\frac{1}{2}\rho V^2}, \qquad [1]$$

where P_3 is the downstream pressure, P_v is the vapour pressure of the water, ρ is the density of the water and V is the average liquid velocity at the orifice.

Cavitation inception was studied under good lighting conditions. Starting from the lowest possible back pressure, the upstream pressure was gradually increased until some very small bubbles could be seen intermittently. These bubbles seemed to form at the vena contracta and were seen at the edge of the submerged liquid jet at and just downstream of the plane of the vena contracta. This condition was defined as cavitation inception, i.e. the first flow regime transition. A slight increase in the downstream pressure causes these small bubbles to disappear. To cause cavitation again, one can either increase the upstream pressure or decrease the downstream pressure.

The results for seven orifices are shown in figure 3. It can be seen that for a given orifice, the cavitation inception number remains constant within a random experimental error with the increase in liquid velocity. Considering the subjective nature of the definition of cavitation inception and human error, the marginal variance is expected. Therefore, it can be concluded that the

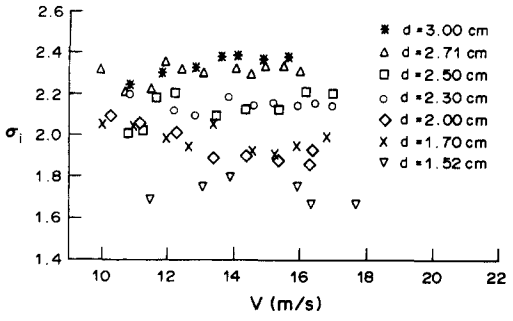

Figure 3. Cavitation inception number (σ_i) vs liquid velocity (V) for seven orifices.

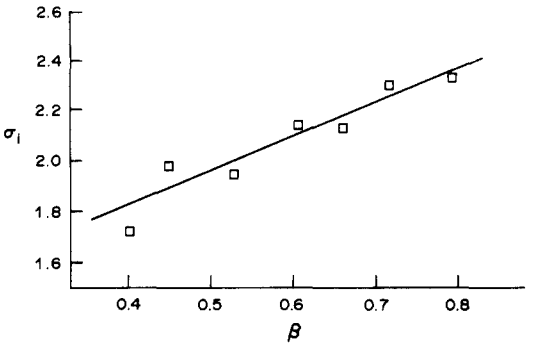

Figure 4. Cavitation inception number (σ_i) vs the diameter ratio (β).

cavitation inception number does not change with the liquid velocity and is a constant for a given orifice.

Figure 4 shows the change of the cavitation inception number with the diameter ratio $\beta\ (=d/D)$. Each point in the figure is the average value taken from figure 3 for a given size or orifice. It can be seen that the cavitation inception number increases approximately linearly with the diameter ratio.

3.2. Comparison with the Literature and Discussion

The results shown above on cavitation inception confirm the conclusion drawn by Numachi *et al.* (1960) and Tullis & Govindarajan (1973) that the cavitation inception number for orifice cavitation is independent of the velocity of the fluid, and of the downstream pressure. Due to the difficulty in reading the data, results from Numachi *et al.* (1960) are shown directly in figure 5. It is evident that the change of σ_i with the downstream pressure P_3 (or the liquid velocity) is only within normal experimental scatter. The cavitation inception number is approximately in the range of 2.0–3.0 for $0.244 < \beta < 0.593$, which is comparable with the present study: σ_i varies between 1.7–2.4 for $0.4 < \beta < 0.8$.

The size scale effect is not obvious in figure 5, though the results from both the present study and Tullis & Govindarajan (1973) indicate that orifice or pipe size has a strong effect on cavitation inception. Figure 6 compares the variation of the cavitation inception number with the diameter ratio β observed in this work and that calculated from Tullis & Govindarajan (1973).† It can be seen that the results from two separate sources show similar trends: the cavitation inception number increases with the diameter ratio. However, the cavitation inception numbers reported by Tullis & Govindarajan (1973) are generally higher than those observed in the present study. This is due to the fact that in the present study the pipe diameter is 3.78 cm, whereas the pipe diameters in their work were 7.8 and 15.4 cm. Therefore we conclude that the cavitation inception number has

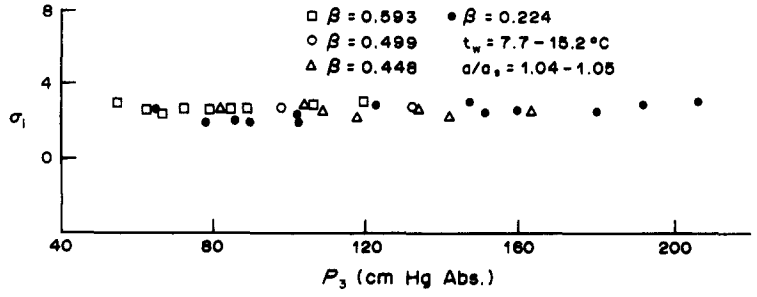

Figure 5. Relation between the cavitation inception (σ_i) and downstream pressure (P_3) [after Numachi *et al.* (1960)].

†It should be noted that Tullis & Govindarajan (1973) defined the cavitation number as $\sigma' = (P_3 - P_v)/(P_1 - P_3)$, which is different from the definition given by [1]. The relation between σ' and σ will be derived later in the paper. Equation [12] has been used to convert σ_i to σ_i'.

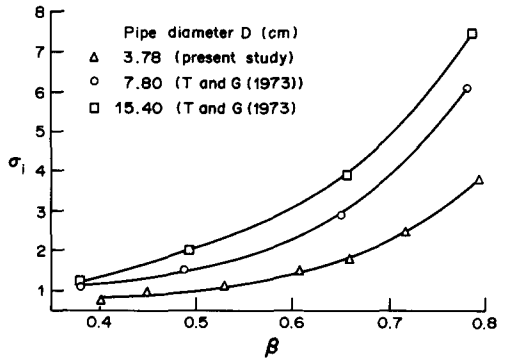

Figure 6. Cavitation inception number (σ_i) vs the diameter ratio (β) for different pipe sizes.

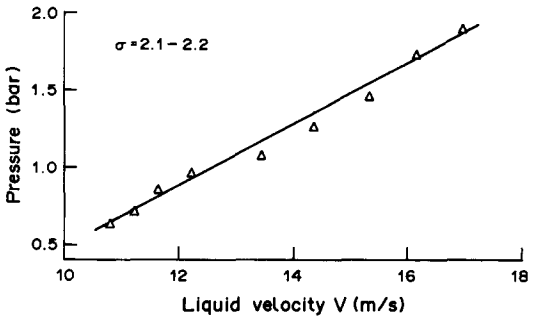

Figure 7. Change in the minimum pressure at cavitation inception with the liquid velocity.

a strong size scale effect, and it is not simply a function of β alone. However, it does not seem to be straightforward to suggest any physical explanation for this.

The minimum pressure at the vena contracta measured at inception is shown in figure 7. It is seen that the pressure is much higher than the vapour pressure ($P_v = 0.0234$ bar at 20°C) and it increases with the liquid velocity, which indicates that at inception, the mechanism of bubble formation is the release of the dissolved gas rather than just the vaporization of the water. (Measurements of the dissolved gas concentration in these experiments are given and discussed in the appendix.) The minimum pressure is therefore not a unique value at inception. Theoretical analyses of bubble growth at cavitation inception using the Rayleigh–Plesset equation (Plesset 1949) and van Wijngaarden's (1967) gas diffusion model have been given by Yan (1989).

4. TRANSITION FROM BUBBLY FLOW TO ANNULAR JET FLOW—CHOKED CAVITATION

4.1. The Prediction of Choked Cavitation

Figures 8(a–h) clearly show the inception and development of cavitation at the orifice. As the cavitation number decreases and the velocity increases, the *white clouds* grow bigger and the length of the cavitation zone extends further downstream from the vena contracta [figures 8(c–e)]. At some critical condition, the vapour close to the wall becomes a continuous phase with some liquid droplets dispersed in it [figure 8(g)]. When this continuous vapour phase first appears it is close to the vena contracta and the cavitation is said to be choked.

The following relation between the flow rate, Q, and the differential pressure across the orifice ($P_1 - P_2$), is well-known:

$$Q = C_d A \sqrt{\frac{2(P_1 - P_2)}{\rho\left(\frac{A^2}{a^2 - 1}\right)}}, \qquad [2]$$

where C_d is the discharge coefficient and A and a are the cross-sectional area of the pipe and the orifice, respectively. In normal operation, when the downstream valve is gradually opened, P_2 is gradually reduced and thus, the flow rate is increased. However, when the (minimum) pressure at the vena contracta reaches its lowest possible value, there will be no further increase in the discharge rate regardless of the decrease in the downstream pressure (P_3). The downstream valve loses its control over the flow.

Obviously, in the present case, the lowest possible value for the minimum pressure is the vapour pressure of the water. (At no stage in these investigations was a pressure significantly lower than the vapour pressure of water measured). Table 1 shows the experimental minimum pressures at the vena contracta when the flow is choked. For each orifice the value is an average from several readings at different velocities. These average values in table 1 for different orifices are close to the value of the vapour pressure of water at room temperature (0.0234 bar). The increase in the

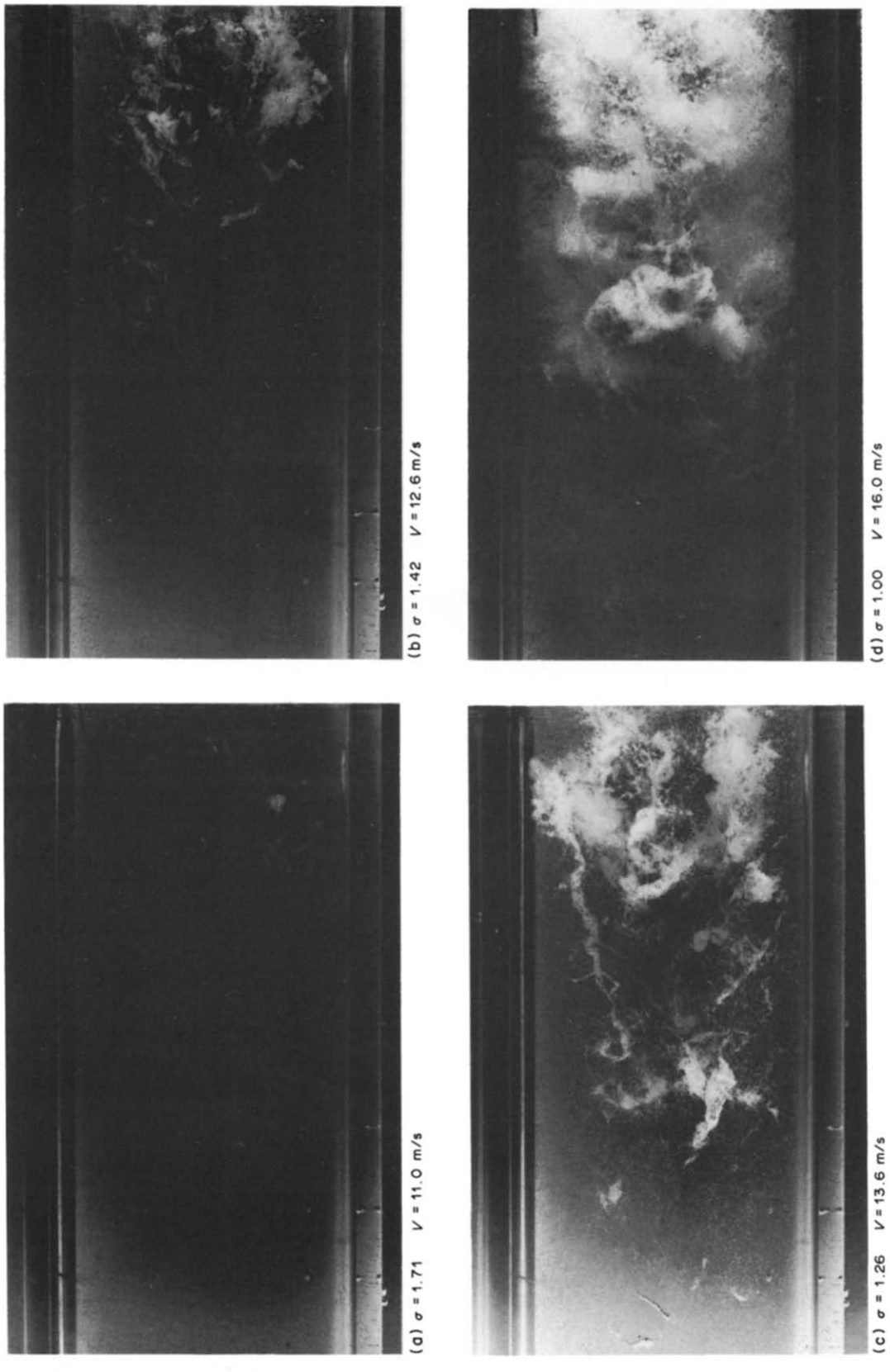
(a) σ = 1.71 V = 11.0 m/s
(b) σ = 1.42 V = 12.6 m/s
(c) σ = 1.26 V = 13.6 m/s
(d) σ = 1.00 V = 16.0 m/s

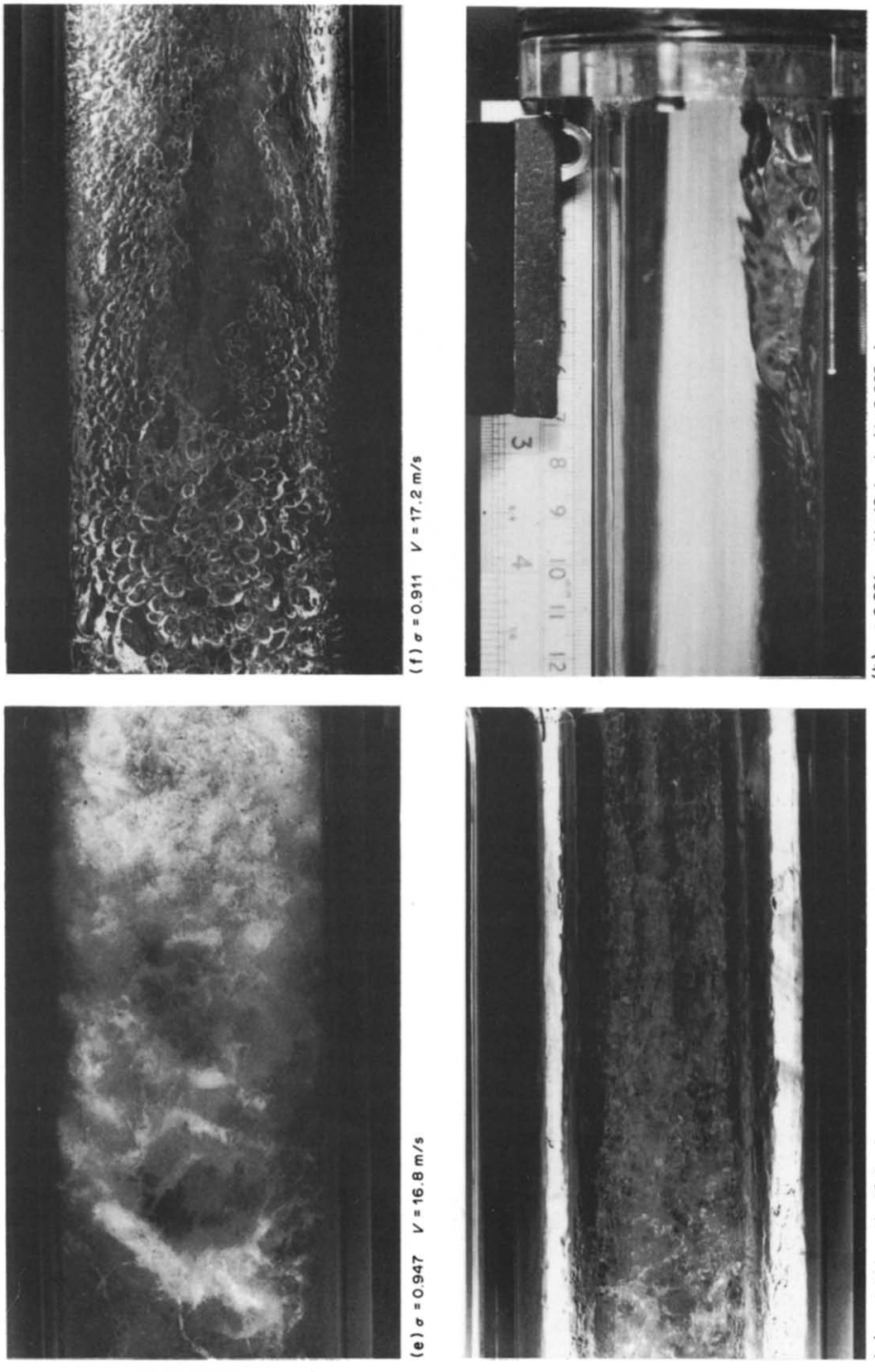

Figures 8(a–h). Photographs showing the development of cavitation downstream of an orifice (flow direction: from right to left).

Table 1. Minimum pressure at choked and super cavitation

d (cm)	P_2(bar)
1.52	0.0281 ± 0.0000
1.72	0.0300 ± 0.0008
2.02	0.0290 ± 0.0011
2.32	0.0292 ± 0.0004
2.50	0.0298 ± 9.0014
2.72	0.0289 ± 0.0007

measured values is due to the release of the dissolved gas and more information will be given below. Based on this condition, a relationship may be derived to predict choked cavitation.

Applying Bernoulli's equation between cross-sections 1 and 2 (figure 1) yields

$$P_1 - P_2 = 0.5\rho\left(\frac{U}{C_d}\right)^2\left(\frac{1}{\beta^4} - 1\right), \quad [3]$$

where U is the mean velocity in the pipe and β is the diameter ratio of the orifice to the pipe (d/D). The equation is essentially identical with [2].

The momentum equation can be applied between cross-sections 2 and 3 to give

$$P_2 - P_3 = U^2\rho\left(1 - \frac{1}{C_c\beta^2}\right), \quad [4]$$

where C_c is the contraction coefficient.

Combining [3] and [4] and noting that $P_2 = P_v$ at choked cavitation, yields

$$\frac{P_3 - P_v}{P_1 - P_v} = \frac{C_d^2\left(\beta^2 - \frac{1}{C_c}\right)}{0.5\left(\beta^2 - \frac{1}{\beta^2}\right)}. \quad [5]$$

Equation [5] indicates that at the flow regime transition from bubbly flow to annular jet flow, the higher the downstream pressure, the higher the upstream pressure has to be. However, the pressure ratio $(P_3 - P_v)/(P_1 - P_v)$ or P_3/P_1 (P_v is small compared with either P_3 or P_1) is a constant for a given orifice, and is independent of the liquid velocity, since C_d and C_c change very little with velocity at high Reynolds number.

The numerical value of the flow coefficient K can be found in the ASME (1959) data book, and the discharge coefficient can therefore be calculated from

$$C_d = K\sqrt{1 - \beta^4}. \quad [6]$$

The value of C_d was measured under a number of experimental conditions and was always found to be in agreement with the value calculated from [6]. The contraction coefficient can be calculated from the following equation (Engel & Stainsby 1964):

$$C_c = \frac{C_d}{\sqrt{1 - \beta^4 + C_d^2\beta^4}}. \quad [7]$$

Equation [5] is plotted in figure 9 for five orifices. For each orifice, a number of different velocities were used. It is evident from the figure that each kind of symbol (from the experiment) essentially follows a straight line (from [5]), which indicates that P_3/P_1 is a constant for a given orifice at the flow regime transition.

Alternatively, P_3 in the momentum equation [4] can be eliminated by combining the momentum equation and [1], the definition of the cavitation number, which leads to

$$P_2 = P_v + V^2\beta^4\rho\left(1 - \frac{1}{C_c\beta^2}\right) + \tfrac{1}{2}\rho V^2\sigma. \quad [8]$$

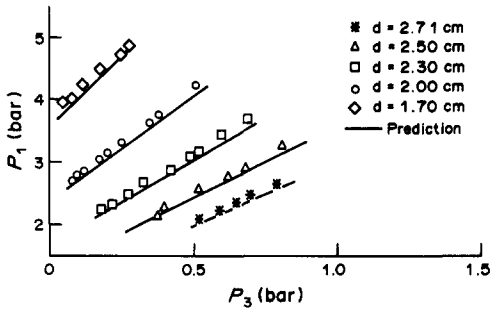

Figure 9. The upstream and the downstream pressure (P_1 and P_3) have a linear relationship at the flow regime transition (choked cavitation) for a given orifice.

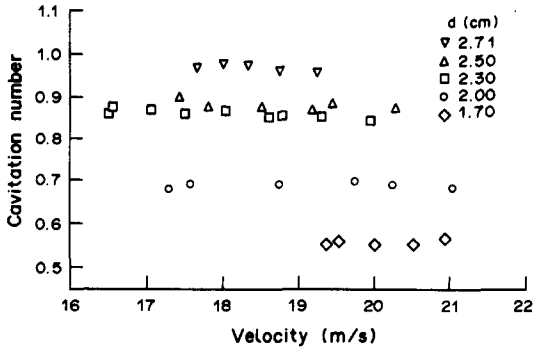

Figure 10. The cavitation number is a constant at the flow regime transition (choked cavitation) for a given orifice.

Again noting that $P_2 - P_v$ at choked flow, we have

$$\sigma = 2\beta^4\left(\frac{1}{C_c\beta^2} - 1\right). \qquad [9]$$

Since C_c is almost independent of the Reynolds number, and β is fixed by the geometry of the orifice and the pipe, the cavitation number is therefore also a constant at the flow regime transition. This conclusion is confirmed by the experimental data shown in figure 10. A comparison may be made between the experiment and the calculated value from [9] and is shown in figure 11. Each of the points is the average taken from figure 10. It is noted that the agreement is good.

4.2. Comparison with the Literature

Tullis & Govindarajan (1973) and Ball *et al.* (1975) also conducted experiments on choked cavitation at an orifice. However, the cavitation number is defined as

$$\sigma' = \frac{P_3 - P_v}{P_1 - P_3}. \qquad [10]$$

The authors calculated the choked cavitation number in the following way. The discharge rate was plotted against the pressure drop ($P_1 - P_3$). Before choked cavitation, the relation between Q and $\log(P_1 - P_3)$ is linear. As soon as the straight line becomes horizontal, i.e. Q remains constant while $P_1 - P_3$ increases, the orifice is choked and the critical value of $P_1 - P_3$ is then determined and the corresponding choked cavitation number is calculated from [10].

Combining the energy equation [3] and the momentum equation [4] yields

$$P_1 - P_3 = \tfrac{1}{2}\rho\left(\frac{U}{C_d}\right)^2\left(\frac{1}{\beta^4} - 1\right) + \rho U^2\left(1 - \frac{1}{C_c\beta^2}\right). \qquad [11]$$

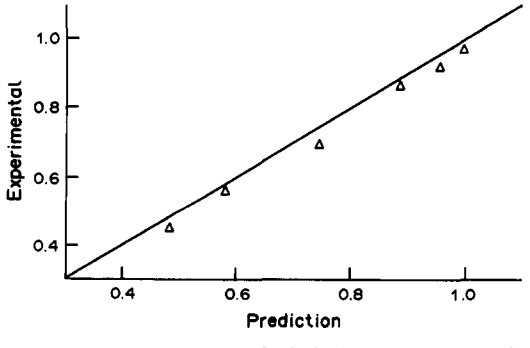

Figure 11. Comparison of choked cavitation numbers between the experimental data and the predicted values according to [9].

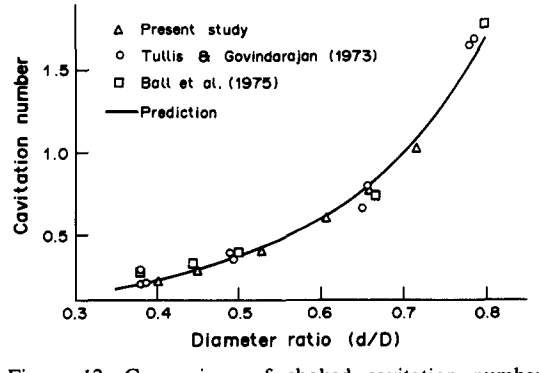

Figure 12. Comparison of choked cavitation numbers between the present study and the literature.

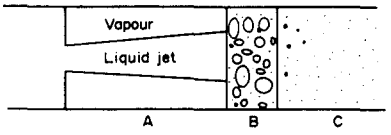

Figure 13. Flow regions at super cavitation: region A—super cavity; region B—white clouds; region C—clear liquid.

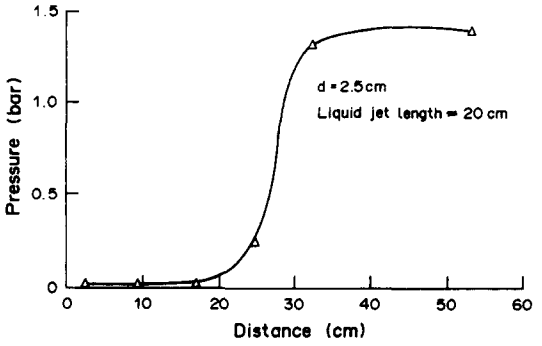

Figure 14. Pressure profile downstream of the orifice at super cavitation.

Substituting $P_1 - P_3$ from this equation, and $P_3 - P_v$ from the cavitation number (see [1]) into [10], we have

$$\sigma' = \frac{\sigma}{\frac{1}{C_d^2}(1-\beta^4) + 2\left(\beta^4 - \frac{\beta^2}{C_c}\right)}. \qquad [12]$$

The choked cavitation number (σ_c), as experimentally determined in the present study, may be substituted into the above equation, and the corresponding value σ_c' can thus be calculated. These values are plotted in figure 12 against β ($=d/D$). Also plotted are the experimental values of δ_c' from the above-mentioned two references (Tullis & Govindarajan 1973; Ball 1975). It is evident that the agreement among the data is very good. The data fit a common curve within the normal experimental scatter. The line represents the predicted value, i.e. from the combination of [9] and [12]. We have thus established a theoretical prediction for the data of other workers who took a purely experimental approach.

It is encouraging to note the following fact regarding the experimental data in figure 12. In the present study, the size of the pipe is fixed. In order to change the value of β, different sizes of orifice were used. However, in the references cited above, the size of the pipe was changed to obtain different values of β. The data in figure 12 indicate that the choked cavitation number has no size scale effect, i.e. it is truly a function of β only, which in this aspect is different from cavitation inception, where there exists a strong size scale effect.

5. SUPER CAVITATION

5.1. Description of the Flow Regions

When super cavitation occurs, the flow downstream of the orifice can be divided into the following distinct regions (figure 13):

Region A—a single cavity with a liquid jet in the middle of a vapour pocket.
Region B—*white clouds* where the big cavity breaks into smaller cavities which collapse. This region appears to be very short, typically 3–5 cm.
Region C—a clear liquid region where all the cavities have collapsed.†

Figure 14 shows a typical pressure profile in super cavitation where the length of the liquid jet is about 20 cm. It is seen that within the jet the static pressure is very low, being close to the vapour pressure of water. In the region in which the bubbles collapse, however, the pressure increases sharply to the pressure that the downstream valve imposes, which is above atmospheric in the present case.

†Though it is called the "clear liquid region", a small amount of dissolved gas is released during cavitation in the form of small gas bubbles. These bubbles exist for some distance before redissolving (see below).

Table 2. Spreading ratio of the liquid jet

d (cm)	2.50	2.30	2.00	1.70	1.52
x_v (cm)	1.89	2.08	2.38	2.65	2.80
C_c	0.653	0.639	0.621	0.610	0.604
d_v (cm)	2.02	1.84	1.58	1.33	1.18
L (cm)	43.8	54.0	58.3	66.5	66.8
α'	0.0210	0.0187	0.0197	0.0192	0.020

Another flow region is particularly noticeable for the biggest orifice, $d = 2.50$ cm. This region exists between regions A and B. The region can be described as the *churn* region. This region looks less *white* than region C, indicating that the collapse of cavities in region C is more severe. The churn regime can extend quite a long distance downstream of the orifice if the downstream pressure is sufficiently low. The condition for the churn regime to appear is that the liquid jet has fully spread to the pipe wall. Due to experimental limitations, not many data points could be obtained for the churn region except for the biggest orifice. It is therefore, not studied separately here but would be worthy of future investigation.

5.2. The Spreading Ratio of the Liquid Jet

From the vena contracta, the liquid jet begins to expand radially and it will eventually spread to the pipe wall which results in a churn region. The spreading ratio of the jet is defined as

$$\alpha' = \frac{d_x - d_v}{2x}, \qquad [13]$$

where d_x is the diameter of the jet at a distance x from the vena contracta and d_v is the diameter of the jet at the vena contracta.

The literature gives no consistent value for the spreading ratio of a free liquid jet, i.e. a jet issued to a free space. Birkhoff & Zarantonello (1957) suggested that the numerical value of the spreading ratio can range from 0.364 to 0.466. Schlichting (1960) and Davies (1972), however, gave much smaller values, i.e. 0.0848 and 0.176, respectively. One common conclusion in the literature is that the spreading ratio of the liquid jet is independent of the jet diameter, or the orifice diameter from which the jet is discharged. In the present study, it was found that the spreading ratio is even smaller. In other words, the jet can travel much further than the calculated distance using the smallest value (0.0848) of the spreading ratio reported in the literature.

The spreading ratio in the present study was determined in the following way. The downstream pressure was sufficiently reduced by opening the downstream valve, that the jet could reach the longest possible length. (Further decrease in the downstream pressure resulted in the churn region.) The maximum jet length is listed in table 2 for the five orifices tested. The distance between the orifice and the vena contracta is determined from ASME (1959). The contraction coefficient can be calculated from [7] and, consequently, the jet diameter at the vena contracta can be calculated. By assuming that the edge of the jet is a straight line, the spreading ratio can be determined. It is seen from table 2 that the average value of the spreading ratio for the different orifices is round 0.02, which is much smaller than the values reported in the literature. Nevertheless, the results in table 2 confirm the conclusion that the spreading ratio does not depend on the orifice diameter. The spreading ratio of the liquid jet is used in the following section.

5.3. Correlation of the Jet Length with Hydraulic Conditions

The jet length is conventionally normalized as

$$L' = \frac{L}{(D - d)}, \qquad [14]$$

where L is the length of the jet from the orifice to the attachment point, i.e. the beginning of the collapse region.

The change of L' with σ is shown in figure 15 for orifices with diameters of 2.50, 2.30, 2.00 and 1.70 cm, respectively. It is seen that the increase in the jet length with the decrease in the cavitation number is almost linear. The change in the jet length with velocity is not regular and is small within

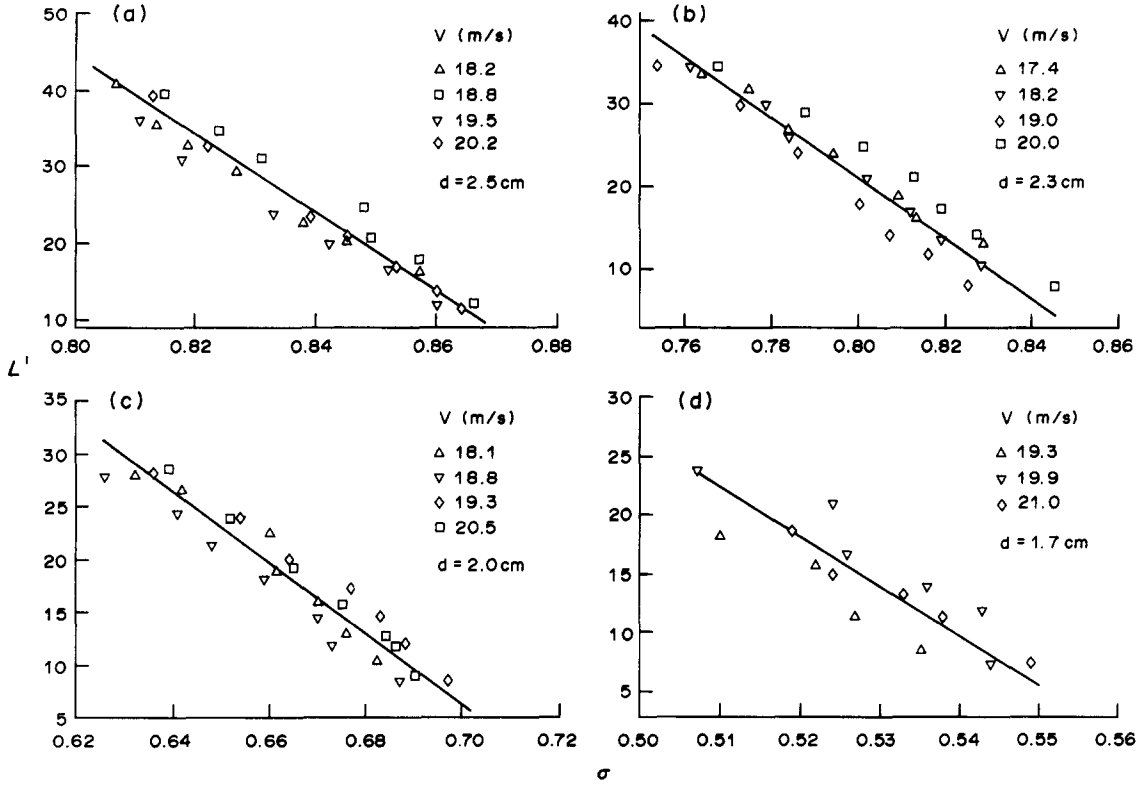

Figures 15(a–d). Correlation of the dimensionless jet length (L') with cavitation number (σ).

the velocity range tested. Thus, it may be suggested that the dimensionless jet length is a function of cavitation number only. Note that in the case of $d = 2.50$ cm, the jet angle is actually the length of the jet plus the length of the churn region whenever the length exceeds the maximum jet length, which is 43.8 cm from the orifice.

5.4. Evaluation of the Vaporization Rate

It is difficult, experimentally, to determine the amount of vapour produced in super cavitation. The vapour produced will all be condensed at the point where the liquid jet ends due to the sudden increase in the pressure. The fact that the jet length increases with the decrease of the downstream pressure implies that more energy is dissipated when the jet is longer. The normal pressure drop (without cavitation) across an orifice is a constant if the velocity does not change, which is obvious from [11]. In super cavitation at a constant velocity, which is fixed by $P_1 - P_2$ [2], the increase in the pressure drop ($P_1 - P_3$) must therefore be due to the increase in the jet length. The method used below to evaluate the vaporization rate is based on this idea, i.e. an energy balance.

It should be noted that the release of the dissolved gas is ignored in super cavitation and only the vaporization of the liquid is considered.

5.4.1. Basic energy loss

The loss of energy at an orifice when there is no cavitation has been studied by a number of investigators (e.g. Lakshmana Rao & Sridharan 1972; Alvi *et al.* 1978; Benedict 1977). Although no details were given about the mechanism of the energy dissipation, it seems obvious that the cause is the inevitable turbulence produced due to the diverging of the flow upon the enlargement in the flow area.

According to Benedict (1977), this energy loss can be expressed in terms of a differential pressure as

$$\Delta P_b = C_e(P_1 - P_2), \qquad [15]$$

where C_e is the energy loss coefficient which can be evaluated from

$$C_e = 1 - \frac{2\beta^2 C_d^2}{(1-\beta^4)}\left(\frac{1}{C_c} - \beta^2\right). \quad [16]$$

We shall call this part of the energy loss, the basic energy loss (ΔP_b). Obviously, in the case of super cavitation, the following additional terms have to be taken into account.

5.4.2. Energy loss due to the collapse of the cavities

At the end of the big cavity, vapour is entrained into the liquid producing smaller cavities which collapse under the downstream pressure P_3. The work done by the external system in completely collapsing the cavities is

$$W = P_3 V_c, \quad [17]$$

where V_c is the total volume of the vapour generated in unit time. Most of this work becomes heat, which may be expressed as an equivalent pressure drop:

$$\Delta P_2 = \frac{W_{irr}}{Q} = \frac{(P_3 - P_v)V_c}{Q}, \quad [18]$$

where W_{irr} designates the irreversible part of W and Q is the volumetric flow rate of the water.

5.4.3. Energy loss due to friction and impact associated with the interface

The formation of the jet results in a two-phase annular flow, and the friction between the vapour phase and the pipe wall is replaced by the friction between the vapour phase and the wall. The velocity difference between the vapour and liquid phase, and the evaporation of mass at the interface cause another extra pressure drop.

A simple model for predicting the interfacial shear in turbulent stratified flow with phase change based on the Reynolds analogy has been proposed by Silver & Wallis (1965/66). According to the model, the shear stress on an interface without phase change is due to some part of the fluid from the main stream striking on the wall and bouncing back again after sharing its momentum with the wall. If a mass ε_0 strikes a unit area per unit time, the shear stress is

$$\tau_0 = \varepsilon_0(v_G - v_L), \quad [19]$$

where v_G and v_L are the gas and fluid velocity, respectively. In a very elementary model, it can be assumed that the mass flux is made up two parts, one moving away from the liquid and the other coming back, each superficially occupying half of the flow area and travelling with average velocity u_0. It is obvious that

$$\varepsilon_0 = \tfrac{1}{2}\rho_G u_0, \quad [20]$$

where ρ_G is the gas/vapour density. If phase change occurs in the interface, and extra mass flux has to be considered. By superimposing a velocity v_G in [20], the mass fluxes leaving and returning to the liquid phase are $\frac{1}{2}\rho_G(u_0 + v_{Gn})$ and $\frac{1}{2}\rho_G(u_0 - v_{Gn})$, respectively (figure 16).

The drag forces acting on the vapour and liquid phase caused by the momentum change are, respectively,

$$F_G = -\zeta(v_G - v_L)\tfrac{1}{2}\rho_G(u_0 + v_{Gn}) \quad [21]$$

and

$$F_L = \zeta(v_G - v_L)\tfrac{1}{2}\rho_G(u_0 - v_{Gn}) \quad [22]$$

where ζ is the perimeter of the interface, i.e. πd_x in the present study, which changes with distance x.

Expressing the above two equations in terms of a mass flux, $m = \rho_G v_{Gn}$, we have

$$F_G = -\zeta(v_G - v_L)\left(\varepsilon_0 + \frac{m}{2}\right) \quad [23]$$

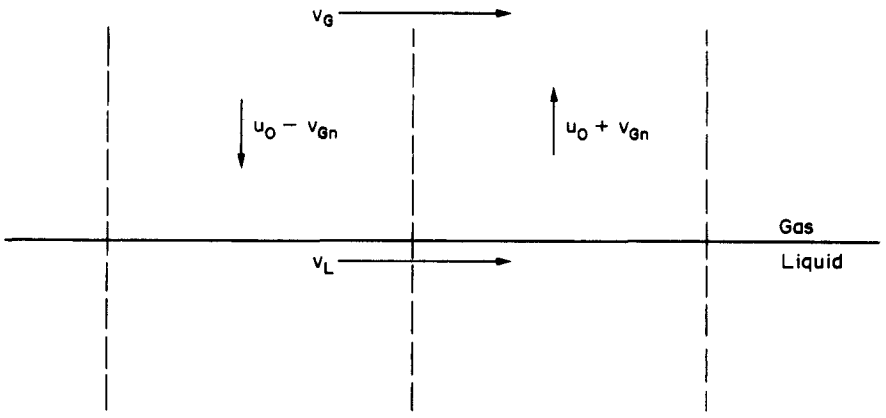

Figure 16. Reynolds analogy with phase change according to Silver & Wallis (1965/66).

and

$$F_L = \zeta(v_G - v_L)\left(\varepsilon_0 - \frac{m}{2}\right). \quad [24]$$

Making use of Wallis' (1960) one-dimensional equations of motion for the two phases, we have

$$\rho_L v_L \frac{dv_L}{dx} = -\frac{dP}{dx} + \frac{\zeta(v_G - v_L)}{A(1-\alpha)}\left(\varepsilon_0 - \frac{m}{2}\right) \quad [25]$$

and

$$\rho_G v_G \frac{dv_G}{dx} = -\frac{dP}{dx} + \frac{F_{w,G}}{\alpha} - \frac{\zeta(v_G - v_L)}{A\alpha}\left(\varepsilon_0 + \frac{m}{2}\right), \quad [26]$$

where: α is the volumetric fraction of the gas and vapour; ρ_G and ρ_L are the density of the liquid and gas phase, respectively; ε_0 is the Reynolds mass flux; m is the vaporizing mass flow rate per unit area of the interface; and $F_{w,G}$ is the friction force between the pipe wall and the vapour phase.

It is obvious from the geometry of the present situation that the perimeter of the interface and the spreading ratio have the following relation:

$$\zeta = \pi(2x\alpha' + d_v). \quad [27]$$

5.4.4. Solving the equations

It is assumed that the vaporization takes place at the surface of the liquid jet and is uniform. In order to determine the value of m, a trial-and-error method was used. For each given value of m, [25] and [26] were integrated over a distance x (the jet length) to give the pressure drop caused by the friction at the interface and at the pipe wall.

The energy loss due to the collapse of the super cavity can be calculated according to [18], where $V_{c,x}$ is equal to the quantity that evaporated in region A upto a distance of x, which can be calculated from

$$V_{c,x} = \int_0^x m\pi(2x\alpha' + d_c)\,dx. \quad [28]$$

The velocity of the vapour and liquid phase at a distance of x in the super cavity region are

$$v_{G,x} = \frac{4V_{c,x}}{4A - \pi d_x^2} \quad [29]$$

and

$$v_{L,x} = \frac{4Q}{\pi d_x^2}. \quad [30]$$

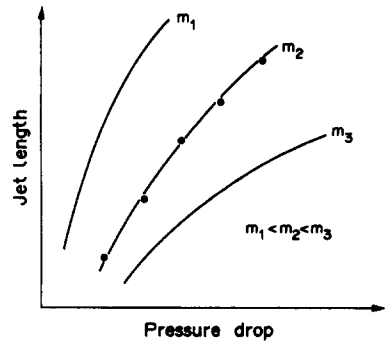

Figure 17. Schematic diagram showing the method of evaluating m.

The friction loss between the vapour phase and the wall, $F_{w,G}$ within the cavity, the friction loss occurring in the collapse region and the clear liquid region as far as the downstream pressure tapping are all calculated from

$$\Delta P = 2c_f \frac{x}{D} \rho u_m^2, \qquad [31]$$

where c_f is the Fanning friction factor and u_m is the average velocity of the vapour or liquid phase. When the Reynolds number based on the pipe diameter, $\mathrm{Re} < 10^5$, the skin friction factor is given by

$$c_f = 0.079\,\mathrm{Re}^{-0.25}. \qquad [32]$$

When $\mathrm{Re} > 10^5$, a linear interpolation method is used based on table 3 from Kay (1963).

The total energy loss (or equivalent pressure drop) therefore consists of the following five parts: (1) basic energy loss [15]; (2) collapsing the cavity [18]; (3) friction at the interface, i.e. at the surface of the liquid jet; (4) friction between the vapour phase and the pipe, region (A); and (5) friction between the liquid phase and the pipe, region C.

The method of evaluating m based on the experiments is illustrated schematically in figure 17. As the value of m is gradually increased, the pressure drop is also increased. At some critical value of m, we have

$$\sum_{i=1}^{N} (\Delta P_e - \Delta P_c)_i^2 \rightarrow \text{minimum}, \qquad [33]$$

where the subscripts e and c mean the experimental and calculated values, respectively, and the sum of i is over a series of experiments.

The evaluation of m from the experimental data is shown in figure 18. It was found that the best fit with the experiments for $d = 2.50$, 2.30, 2.00 and 1.70 cm corresponds to $m = 1.12$, 1.02, 0.951 and 0.945 g/m^{2}s. The difference between the values of m is small and can be regarded as independent of the orifice size.

A numerical example is supplied here. As water passes through an orifice of $d = 1.7$ cm in a pipe of $D = 3.78$ cm, with $U = 3.89$ m/s, a jet of length 26.2 cm is created. When the best fit is achieved i.e. $m = 0.945$ g/m^{2}s, the rate at which water is vaporized is $G_m = 0.0142$ g/s. The average velocity of the vapour phase based on the pipe area at the end of the jet is 0.73 m/s.

It should be noted that the calculations for $d = 2.5$ cm stop at about 40 cm. The maximum jet length is 43.8 cm and beyond that is the churn region. As the jet length approaches the maximum value, the flowing area for the vapour phase approaches zero. Thus, the pressure drop increases extremely quickly with the increase in the jet length, and the lines begin to deviate sharply from the data. This condition can be regarded as the limit of the model.

Table 3. Skin friction coefficient (Kay 1963)

Re ($\times 10^5$)	1	2	5	10	20	50
c_f	0.00449	0.00391	0.00329	0.00292	0.00260	0.00226

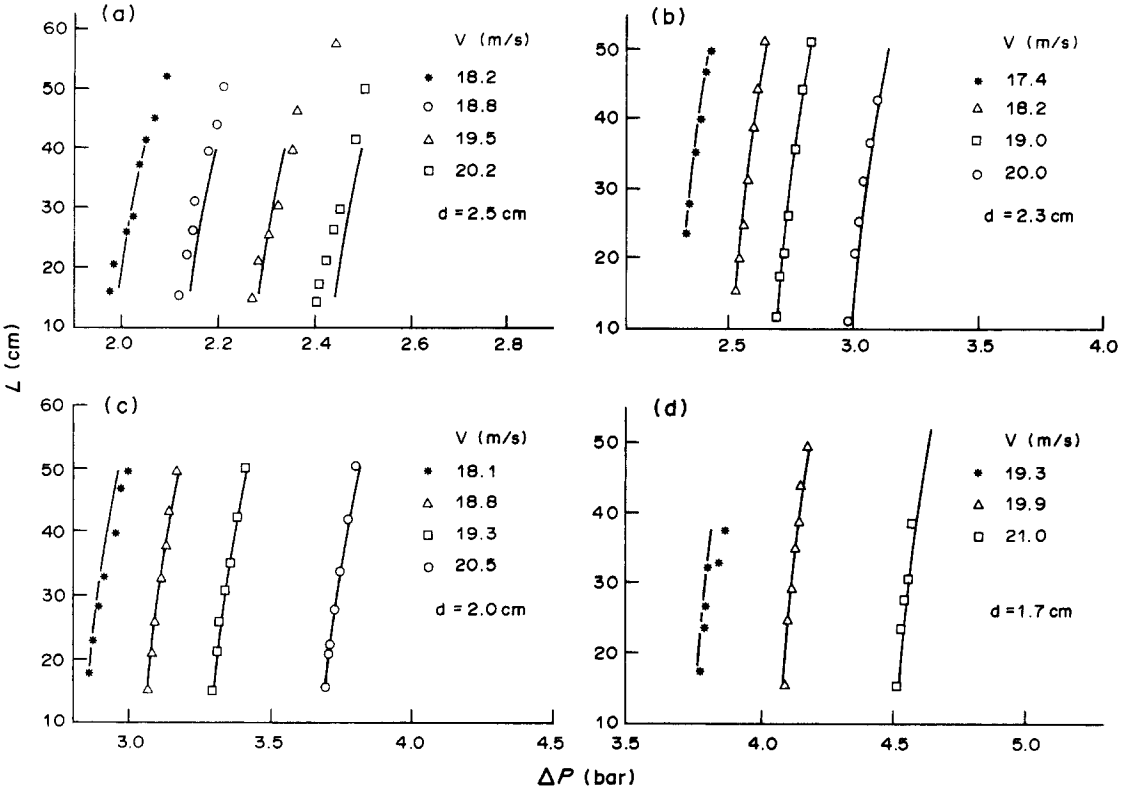

Figures 18(a–d). Evaluation of the vaporizatite (m) based on experiments: the symbols indicate experimental results; the lines are from trial-and-error solutions.

5.4.5. Comments and discussion

In applying the Reynolds flux model to evaluate m, it is assumed that the vaporization on the surface of the jet is uniform. In practice, however, this might not be true. From the view point of heat transfer, the vaporization rate will probably gradually decrease as the jet travels downstream, since the temperature of the jet surface will certainly be reduced due to the vaporization.

It has generally been believed that it is difficult to predict the jet length in super cavitation (Tullis 1971 etc.). However, once the value of m is obtained, the method used above can in turn be used to predict the jet length in super cavitation, since m is approximately independent of the geometry. The effect of pipe size has not been investigated.

It should be emphasized that the value of m should be dependent on the liquid temperature, and probably the content of the dissolved gas as well. Both these factors have been left for future consideration in the present study.

6. THE FORCED FLOW REGIME TRANSITION—AIR INTRODUCTION

The idea of introducing air to the cavitation zone to reduce cavitation noise and damage has long been reported (e.g. Mousson 1937 etc.). It has been found in the present study that air introduction can not only suppress cavitation (Yan *et al.* 1988) but can also cause a flow regime transition from bubbly flow to annular concurrent jet flow. The amount of air needed to cause this flow regime transition depends on the cavitation number, i.e. the severity of cavitation. Further analysis leads to some very useful and interesting results regarding choked cavitation, the second stage transition of the flow regime.

6.1. Critical Air Flow Rate

As the flow rate is gradually increased, separation or detachment of bubbly flow from the orifice is observed. When the air flow rate increases to a certain value, the separation becomes stable: the flow regime looks the same as in choked cavitation. We shall refer to this value as the critical

air flow rate. If the flow rate exceeds this critical value, the annular region will extend further downstream and the position of the end of this region may oscillate significantly. Such oscillations have a much smaller amplitude in the case of super cavitation without air injection, and this fact suggests that the rate of air injection in these experiments was less steady than the rate at which dissolved gas is released in the super cavitation experiments. This oscillatory behaviour may be compared with the instability of a ventilated cavity behind a bluff body, which has been studied by a number of investigators (e.g. Silberman & Song 1961; Song 1962; Woods 1966 etc.).

The critical air flow rate is shown in figures 19(a–d) for orifices of $d = 2.50$, 2.32, 2.02 and 1.72 cm at different velocities. In the figure the solid symbols correspond to natural suction, i.e. air was drawn into the low pressure zone from atmospheric pressure, whereas the open symbols correspond to *forced* injection in which the air pressure upstream of the nozzles was 0.75 bar gauge. It is evident that, at a fixed cavitation number, more air is required to cause the flow regime transition at higher velocities. On the other hand, the critical air flow rate and the cavitation number follow a linear relation at a constant velocity. It is interesting to note that when the cavitation number is reduced to a critical value, which is only possible at high velocities in the present apparatus, no air is needed to cause the flow regime transition. This condition coincides with choked cavitation as discussed above. The conclusion that the choked cavitation number is a function of the diameter ratio β only (see [9]) is confirmed here since all the straight lines (at different velocities) in the figure meet at one point as the cavitation number decreases to acritical value. The choked cavitation number, i.e. the origin of the straight lines in each part of the figure, is shifted towards a smaller value as the orifice diameter decreases, which can also be predicted according to [9].

If the measured critical air flow rate is expressed in volumetric terms at the pressure behind the orifice, P_2, it is interesting to note that the flow rate appears to be a constant at any cavitation numbers for a given velocity [figures 20(a–d)]. This idea is mostly based on the data, and seems to be more justified at high cavitation numbers where cavitation does not complicate the flow, e.g. the points for $V = 6.58$ and 9.03 m/s [△ and ○ symbols in figure 20(a)]. Here the cavitation number

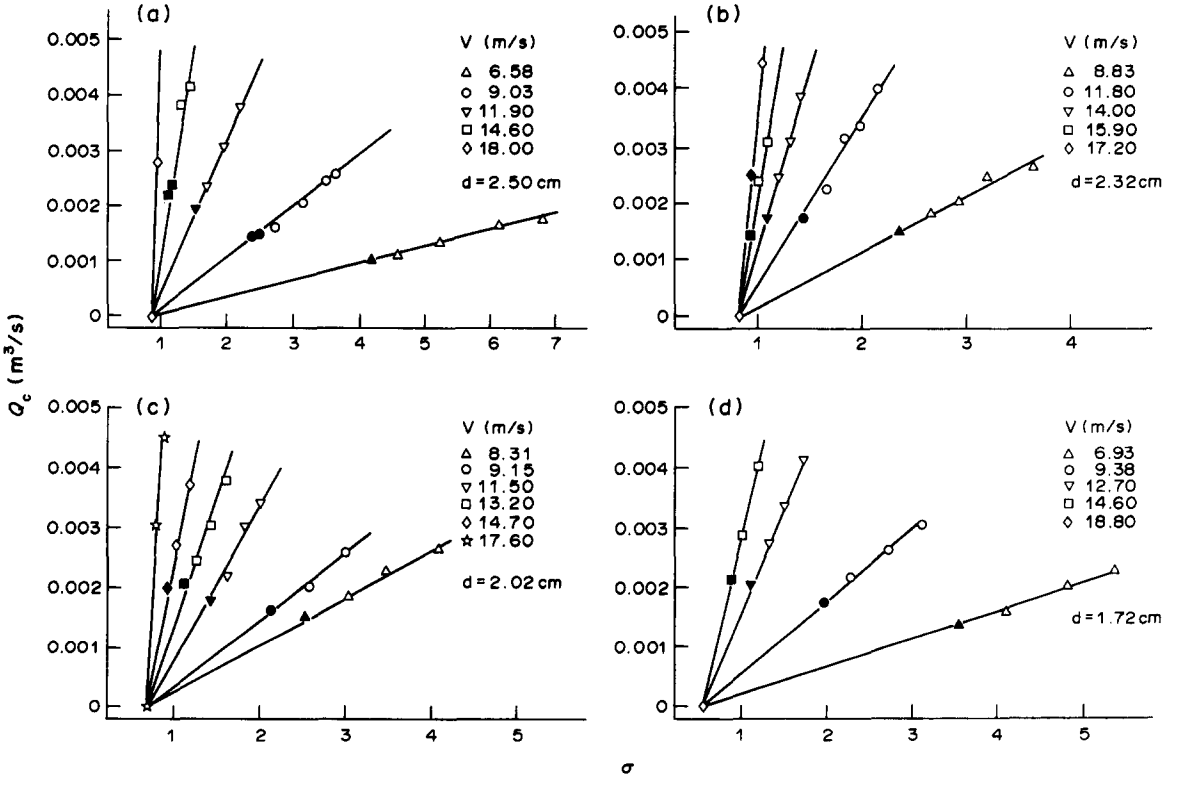

Figures 19(a–d). Change in the critical air flow rate Q_c with the hydraulic conditions (solid symbols for natural suction and open symbols for forced injection).

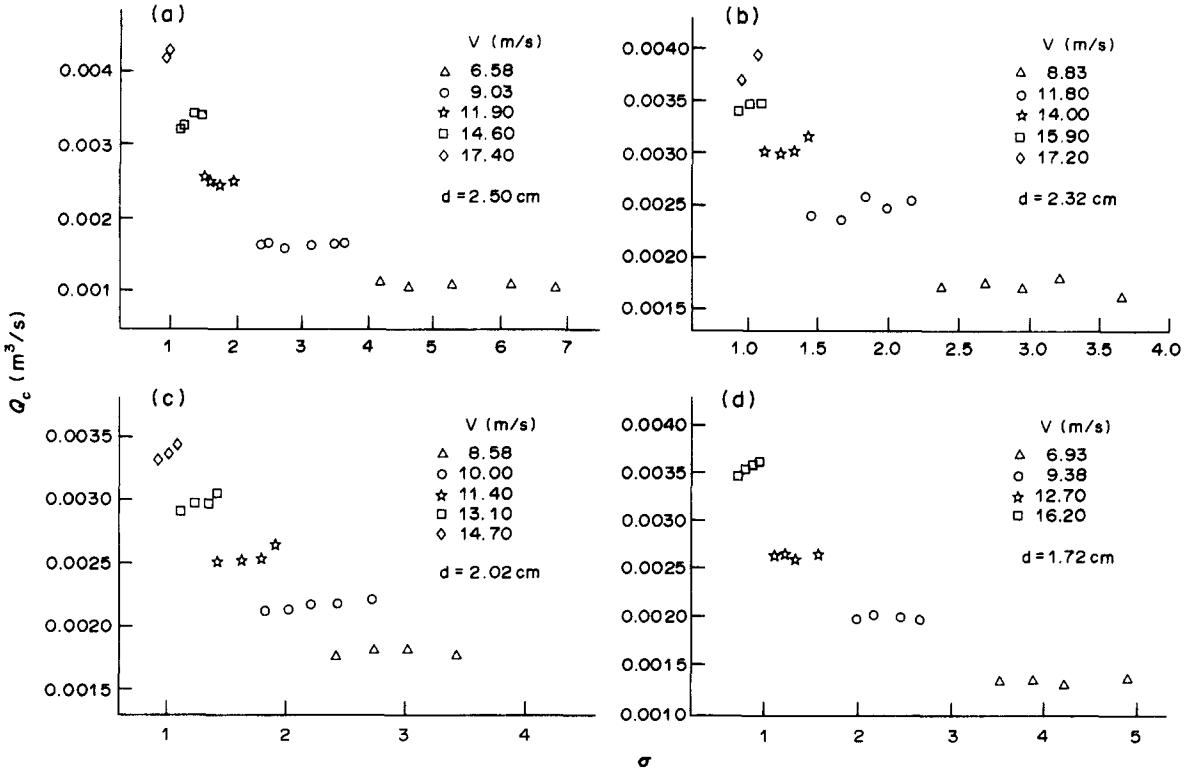

Figures 20(a–d). Change in the critical air flow rate Q_c (at P_2) with hydraulic conditions.

spans a wide range. At a fairly low cavitation number, the flow itself produces a certain amount of vapour and gas due to cavitation and consequently the amount of air needed to cause the flow regime transition tends to decrease. However, it might be suggested from the above evidence that, at any cavitation number the total amount of gas and vapour produced due to cavitation, plus the introduced air under P_2, is a constant at the flow regime transition. This provides an interesting way of determining the flow rate of the vapour and the released gas during cavitation at the choked condition. Here is an example. In figure 19(a) ($d = 2.50$ cm), at $V = 9.03$ m/s, when the cavitation number is reduced to about 0.9, choked cavitation occurs: no air is needed to cause the flow regime transition. When the cavitation number is increased to about 2.4, no cavitation bubbles are observed. In order to cause the flow regime transition at this cavitation number, the required air flow rate (at P_2) is approx 1.65×10^{-3} m³/s [figure 20(a)]. Consequently, the total amount of vapour and gas released when the flow is choked ($\sigma_c \approx 0.9$) at the same velocity is also 1.65×10^{-3} m³/s (at P_2).

6.2. *Correlations and Discussion*

6.2.1. *Correlations*

Figure 21 shows the manner in which the critical air flow rate under P_2 changes with the liquid velocity for the four orifices investigated. Each individual point is the average for different cavitation numbers but at the same velocity as in figures 20(a–d). It is surprising to note that: (i) by using the average velocity at the orifice, the air flow rates under P_2 are well-correlated for different orifices; and (ii) the flow rate and the liquid velocity have an excellent linear relationship. It is found (by least squares) that the best straight line through the data obeys the following equation:

$$Q_c = 0.268 \times 10^{-3} V - 0.652 \times 10^{-3}, \qquad [34]$$

where Q_c denotes the critical air flow rate and the constants have units of m² and m³/s, respectively.

Hence for any size of orifice at any cavitation number, the critical volumetric air flow rate (at P_2) can be determined according to the equation which depends on the average liquid velocity at the orifice only.

As mentioned earlier, once choked cavitation occurs the minimum pressure in the cavitation zone must drop close to the vapour pressure of the liquid. From our experimental results the pressure (P_2) at choked flow is slightly higher than the vapour pressure due to the released gas originally dissolved in the liquid. The typical increase is around 0.006 bar at room temperature (20°C), at which our experiments were carried out, i.e. $P_{min} = P_v + P_G$ where P_G is the partial pressure of the released gas. Assuming that the gas released obeys the ideal gas law, it is readily shown that at the choked condition the gas flow rate due to cavitation expressed as a volumetric flow rate at atmospheric temperature and pressure is given by

$$Q_G = \frac{P_G}{P_{atm}} Q_c. \qquad [35]$$

Taking $P_G = 0.006$ bar, as seems to be true for all the present experiments, and $P_{atm} = 1.013$ bar and substituting Q_c into the equation, we have

$$Q_G = 1.59 \times 10^{-6} V - 3.86 \times 10^{-6}, \qquad [36]$$

where the numerical constants have units of m^2 and m^3, respectively. The released gas flow rate is therefore a function of the liquid velocity only. The mass flow rate of the vapour is given by the law of partial pressures:

$$M_v = \left(\frac{P_v}{P_v + P_G}\right) Q_c \rho_v, \qquad [37]$$

where ρ_v is the density of the vapour at room temperature. Substituting Q_c into the equation and take ρ_v as 0.0173 kg/m^3 (at 20°C), the equation becomes

$$M_v = 3.71 \times 10^{-6} V - 9.03 \times 10^{-6}, \qquad [38]$$

where the numerical constants have units of kg/m and kg/s, respectively.

6.2.2. Discussion

A closer examination of figure 21 reveals that the slope for the largest orifice is slightly greater than that for the smallest orifice. However, the difference is negligible within the range of β in the present study, i.e. from 0.455 to 0.661. Consequently, all the correlations presented above are subject to the same condition. As β approaches 0 or 1, the difference between the slopes in figure 21 can be very large and the correlations cannot be expected to hold true. The same restrictions apply to the liquid velocity V. Equation [34] makes no sense when $V \leqslant 2.43$ m/s. Therefore, the correlations should be used with great caution outside the range of experimentation.

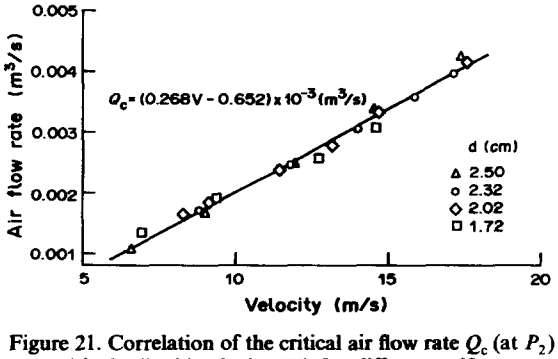

Figure 21. Correlation of the critical air flow rate Q_c (at P_2) with the liquid velocity (V) for different orifices.

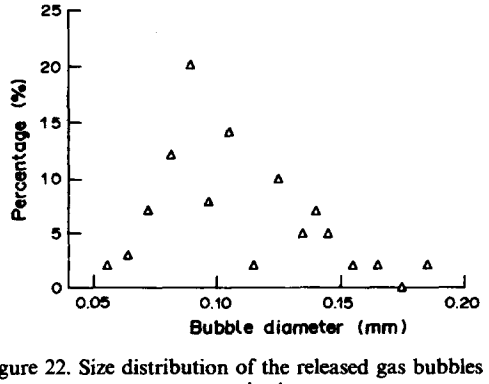

Figure 22. Size distribution of the released gas bubbles due to cavitation.

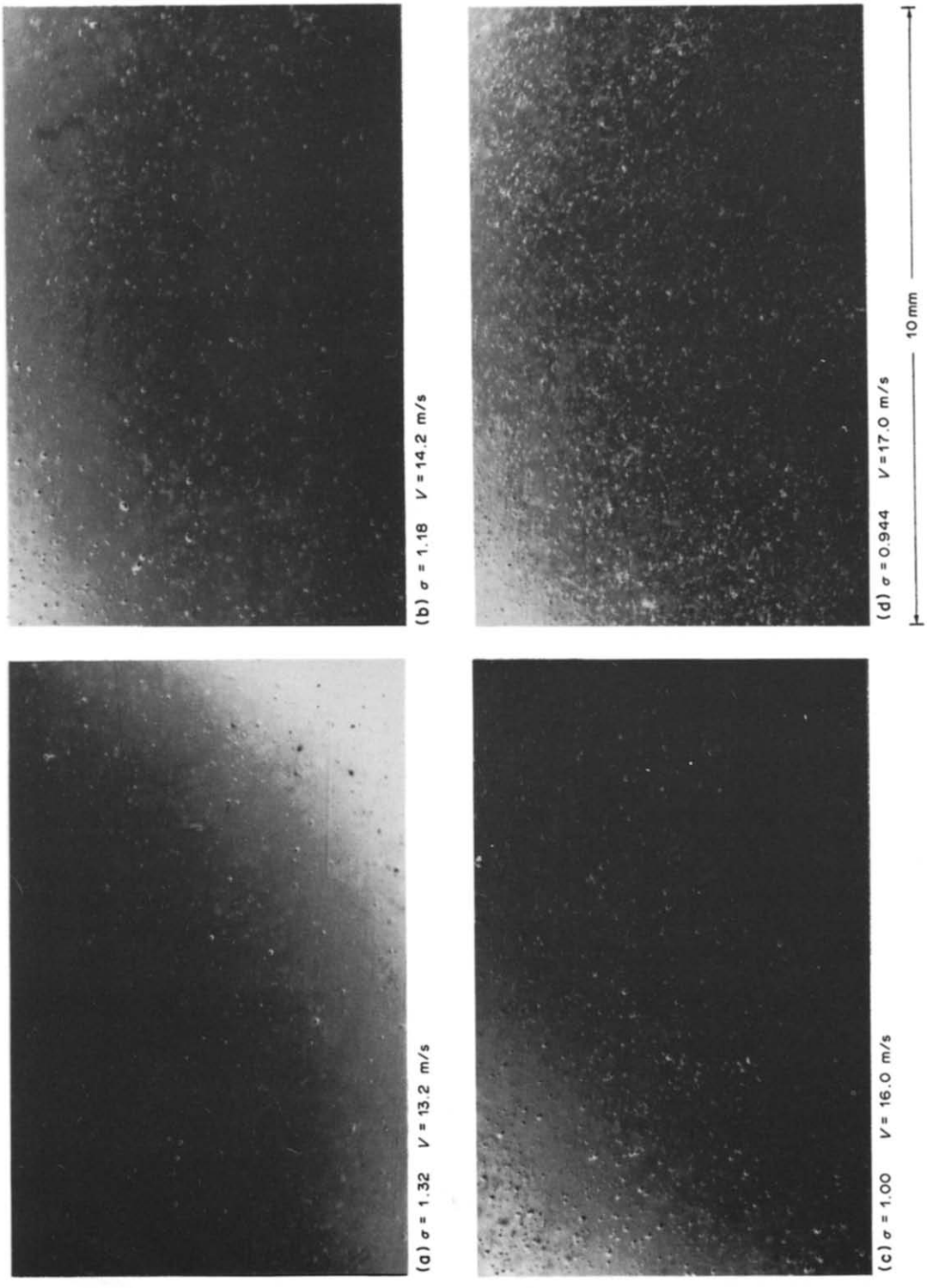

Figures 23. Gas bubbles produced due to cavitation.

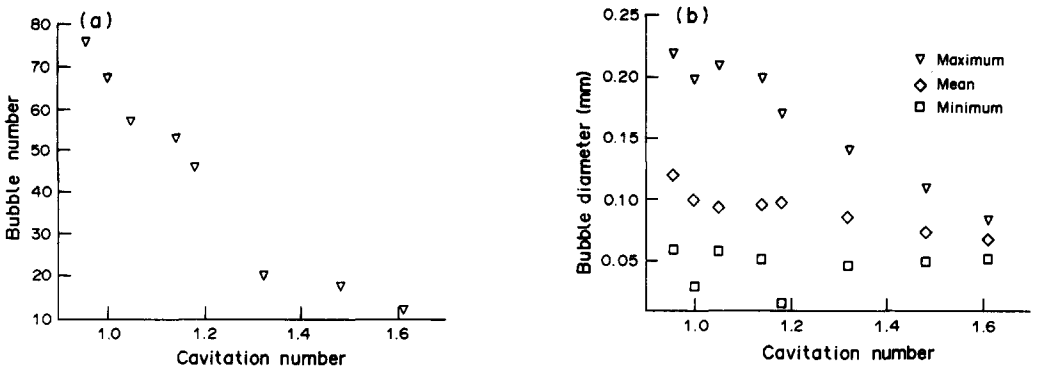

Figures 24(a, b). Change in the number (a) and size (b) of the released gas bubbles with cavitation number.

6.3. The Size of the Released Gas Bubbles

The released gas bubbles can be easily seen far downstream of the orifice, where the pressure has fully recovered. Photographs have been taken 0.33 m downstream of the orifice and the films have been analysed using an Optomax image analyser. A typical size distribution of the bubbles is shown in figure 22, where $\sigma = 0.944$ and $V = 17.0$ m/s. It is noted that the bubble size ranges from 0.05 to 0.18 mm in diameter and the highest concentration of the bubbles is around 0.11 mm. Several photographs are shown in figures 23(a–d). It is seen that the bubbles are spherical and the number of bubbles is increased as cavitation becomes more and more severe. Figure 24(a) shows the change in the bubble density with the cavitation number within the focus range; figure 24(b) shows the change in the maximum, mean and minimum bubble diameter. It is obvious that all these parameters are increased as the cavitation number decreases.

7. CONCLUSIONS

The results for the two stages of the flow regime transition have been presented and discussed. The first stage, called cavitation inception, from single-phase to two-phase bubbly flow is independent of the liquid velocity. However, the cavitation number at this transition is not a simple function of β. It has a strong size scale effect, i.e. it increases with the size of the pipe. The minimum pressure at inception is well above the vapour pressure and it increases with the liquid velocity. The formation of small bubbles at inception is due to gas release upon pressure reduction. The second stage transition from bubbly flow to annular jet flow corresponds to the choked condition which leads to super cavitation. Choked cavitation occurs when the minimum pressure drops to the vapour pressure of the flowing liquid and it can be predicted according to [5] in terms of a pressure ratio [9] in terms of the cavitation number. Vaporization of the liquid becomes dominant at choked and super cavitation.

It has been found, in super cavitation, that the dimensionless jet length can be correlated by using the cavitation number, and the relation between the two dimensionless parameters is approximately linear. The vaporization rate of the surface of the liquid jet has been evaluated based on the experimental data. The dependence of m upon the orifice size is small. A value of 1 g/m^2 s independent of the orifice size gives a reasonable fit to the data. It may be suggested that this value of m can be used to predict the jet length in super cavitation once the value of m is determined under laboratory conditions.

Air admittance can also cause flow regime transition from bubbly flow to annular flow. The transition can be brought about either by natural suction or by forced injection. When the cavitation number is reduced to the choked value, which is a constant for a given β ratio, no air is needed to cause the transition. The critical volumetric air flow rate at P_2 is a function of the liquid velocity (V) only and is independent of the cavitation number. The correlation of the critical air flow rate with the average liquid velocity at the orifice seems independent of the orifice size within the tested range in the present study. The amount of vapour and released gas at choked cavitation (second stage transition) can be estimated from the correlations in this paper.

REFERENCES

ALVI, S. H., SRIDHARAN, K. & LAKSHMANA RAO, N. S. 1978 Loss characteristics of orifices and nozzles. *Trans. ASME J. Fluids Engng* **100,** 299–307.

ASME, 1959 *Fluid Meters—Their Theory and Application*, 5th edn. ASME, New York.

BALL, J. W., TULLIS, J. P. & STRIPLING, T. 1975 Predicting cavitation in sudden enlargement. *J. Hydraul. Div. ASCE* **HY17,** 857–870.

BENEDICT, R. P. 1977 Loss coefficients for fluids meters. *Trans. ASME J. Fluids Engng* **99,** 245–248.

BIRKHOFF, G. & ZARANTONELLO, E. H. 1957 *Jet, Wakes, and Cavities*. Academic Press, New York.

DAVIES, J. T. 1972 *Turbulent Phenomena*. Academic Press, New York.

ENGEL, F. V. A. E. & STAINSBY, W. 1964 Discharge coefficient characteristics of orifices. *Engineers* **218,** 161–168.

KAY, J. M. 1963 *An Introduction to Fluid Mechanics and Heat Transfer*. Cambridge Univ. Press, Cambs.

LAKSHMANA RAO, N. S. & SRIDHARAN, K. 1972 Orifice losses for laminar approach flow. *J. Hydraul. Div. ASCE* **HY11,** 2015–2034.

MOUSSON, J. M. 1937 Pitting resistance of metals under cavitation conditions. *Trans. ASME* **59,** 399–408.

NUMACHI, F., YAMABE, M. & OBA, R. 1960 Cavitation effect on the discharge coefficient of the sharp-edge orifice plate. *Trans. ASME J. bas. Engng* **8,** 1–11.

PLESSET, M. S. 1949 The dynamics of cavitation bubbles. *Trans. ASME J. appl. Phys.* **25,** 228–231.

SCHLICHTING, H. 1960 *Boundary Layer Theory*, 4th edn. McGraw-Hill, New York.

SILBERMAN, E. & SONG, C. S. 1961 Instability of ventilated cavities. *J. Ship Res.* **5,** 13–33.

SILVER, R. S. & WALLIS, G. B. 1965/66 A simple theory for longitudinal pressure drop in the presence of lateral condensation. *Proc. Instn mech. Engrs* **180,** 36–42.

SONG, C. S. 1962 Pulsation of two-dimensional cavities. In *Proc. 4th Symp. on Naval Hydrodynamics*. Report ONR/ACR-92, pp 1033–1056.

TULLIS, J. P. 1971 Choking and supercavitating valves. *J. Hydraul. Div. ASCE* **HY12,** 1931–1945.

TULLIS, J. P. & GOVINDARAJAN, R. 1973 Cavitation and size scale effect for orifices. *J. Hydraul. Div. ASCE* **HY13,** 417–430.

VAN WIJNGAARDEN, L. 1967 On the growth of small cavitation bubbles by convective diffusion. *Int. J. Heat Mass Transfer* **10,** 127–134.

WALLIS, G. B. 1960 *One-dimensional Two-phase Flow*. Academic Press, New York.

WOODS, L. C. 1966 On the instability of ventilated cavities. *J. Fluid Mech.* **26,** 437–457.

YAN, Y. 1989 Cavitation phenomena and the effect of the admittance of air in the flow through an orifice. Ph.D. Dissertation, Univ. of Cambridge, Cambs.

YAN, Y., THORPE, R. B. & PANDIT, A. B. 1988 Cavitation noise and its suppression by air in orifice flow. In *Proc. Int. Symp. on Flow-induced Noise and Vibration, Chicago, Ill.* (Edited by KEITH, W. L., URAM, E. M. & KALINOWSKI, A. J.), Vol. 6, pp. 25–39. ASME, New York. Vol. 6, pp. 25–39.

APPENDIX

The Dissolved Gas Concentration

During the main experimentation reported in this paper no measurements were made of the amount of permanent gas dissolved in the water which was being used: it was assumed that this would be close to the amount in equilibrium with air at atmospheric pressure. It is clear from the reproducibility of the experimental results that no significant departures from this state of affairs is likely to have occurred. However, after the main experiments had been concluded, an investigation of the dissolved oxygen concentration was undertaken.

Dissolved oxygen probes are commercially available for use with biological fermentations and digestions. Such a probe was calibrated and used to measure the oxygen concentration in samples of water taken from the cavitation apparatus a short distance upstream of the orifice plate.

Running the apparatus at cavitation numbers higher than that which characterizes cavitation inception gave dissolved oxygen concentrations 10–20% higher than equilibrium at atmospheric

pressure and this may be attributed to a small number of bubbles being entrained into the pump and dissolving in the high-pressure water before reaching the orifice plate.

Running the apparatus at cavitation numbers between that which characterizes inception and that which characterizes the transition to super cavitation gave similar dissolved oxygen concentrations, i.e. 10–20% higher than equilibrium.

Running the apparatus in a super cavitation mode caused the dissolved oxygen concentration to drop at a rate of about 1%/min. This drop in concentration may be attributed to the formation of large numbers of cavities which contain a significant proportion of dissolved gas, part of which remains in the gas phase as small bubbles even after the collapse of the cavities: as is noted in the main text, such bubbles were observable. A decay in dissolved gas concentration of 1%/min constitutes a rate which, whilst casting some doubt on the exact value in each experiment, leads us to believe that the actual concentration was never more than 20% greater or (less likely) less than that which is equilibrium value for air and water at a total pressure of 1 bar.

It is clear from our experiments that the dissolved gas is of some importance in cavitation and that it is worthy of greater and more careful consideration.